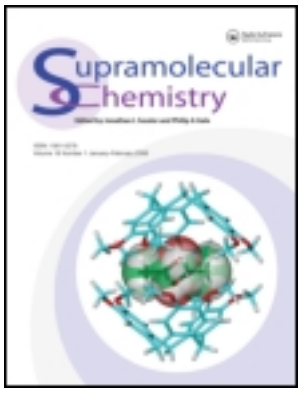

Supramolecular Chemistry
Publication details, including instructions for authors and subscription information:
http://www.tandfonline.com/loi/gsch20

# Theoretical studies on the structural and magnetic property of arginase active site

Toru Saito [a], Yusuke Kataoka [a], Yasuyuki Nakanishi [a], Yasutaka Kitagawa [a], Takashi Kawakami [a], Shusuke Yamanaka [a], Mitsutaka Okumura [a] & Kizashi Yamaguchi [a]
[a] Department of Chemistry, Graduate School of Science, Osaka University, 1-1 Machikaneyama, Toyonaka, Osaka, 560-0043, Japan

Available online: 27 Aug 2010

To cite this article: Toru Saito, Yusuke Kataoka, Yasuyuki Nakanishi, Yasutaka Kitagawa, Takashi Kawakami, Shusuke Yamanaka, Mitsutaka Okumura & Kizashi Yamaguchi (2011): Theoretical studies on the structural and magnetic property of arginase active site, Supramolecular Chemistry, 23:01-02, 22-28

To link to this article: http://dx.doi.org/10.1080/10610278.2010.506552

*Supramolecular Chemistry*
Vol. 23, Nos. 1–2, January–February 2011, 22–28

Taylor & Francis
Taylor & Francis Group

# Theoretical studies on the structural and magnetic property of arginase active site

Toru Saito*, Yusuke Kataoka, Yasuyuki Nakanishi, Yasutaka Kitagawa, Takashi Kawakami, Shusuke Yamanaka, Mitsutaka Okumura and Kizashi Yamaguchi

*Department of Chemistry, Graduate School of Science, Osaka University, 1-1 Machikaneyama, Toyonaka, Osaka 560-0043, Japan*

(*Received 31 May 2010; final version received 20 June 2010*)

The chemical species of solvent molecule (WB) between two manganese ions in the active site of arginase is investigated based on the structural and magnetic property. The calculated magnetic coupling constant ($J_{ab}$) values at UBH&HLYP level of theory are $-1.9\,cm^{-1}$ for WB = $H_2O$ and $-5.7\,cm^{-1}$ for WB = $OH^-$, respectively. In comparison with the experimental value ($J_{ab} = \sim -2.0\,cm^{-1}$), $H_2O$ is the most likely candidate to WB in the initial structure. Natural orbital analyses reveal that WB plays an important role for keeping the geometry of the Mn–O(WB)–Mn core rigid rather than mediating superexchange interaction. The result indicates that WB does not have to shift to one Mn ion as an initiation of the hydrolysis reaction.

**Keywords:** word; DFT; magnetic coupling constant; manganese



## 1. Introduction

Arginase catalyses the hydrolysis of L-arginine to form L-ornithine and urea in the liver (*1*). According to the X-ray crystallographic structure (PDB code: 1RLA), rat liver arginase is a homotrimer, and each active site consists of binuclear Mn(II)–Mn(II) cluster (*2*). The two manganese ions Mn(II)–Mn(II) are located at the bottom of an active site cavity, and their separation is 3.3 Å. The solvent molecule (WB) bridges both Mn ions, and each Mn–O(WB) distance is 2.4 Å. It agrees with the EPR spectrum that supports the $\mu$-ligand bridge spin-coupled Mn–O(WB)–Mn core (*3*). EPR measurements of wild-type arginase reveal antiferromagnetic coupling between Mn ions with small exchange coupling constant ($J_{ab} = \sim -2.0\,cm^{-1}$) (*4*,*5*).

The mechanism of hydrolysis reaction has been investigated by mutagenesis approaches and EPR studies with various inhibitors of rat arginase (*2*–*10*). These studies revealed that the bridging species (water molecule or hydroxyl group) plays an important role of the hydrolysis. Dismukes and his co-workers (*4*,*5*) pointed out that chemical species of WB should be $\mu$-$H_2O$ rather than $\mu$-$OH^-$ judging from small $J_{ab}$ value. They also showed that the magnetic interaction between two manganese ions disappears when adding *N*ω-OH-L-arginine (NOHA) as an inhibitor. Based on these behaviours, they proposed that the cleavage of one of Mn–O bonds was assumed to lead nucleophilic attack after the superexchange interaction in the Mn–WB–Mn core is abolished. On the other hand, Christianson and his co-workers (*2*,*9*,*10*) proposed that metal-activated bridging $OH^-$ attacks the substrate by transferring proton to leaving group via Asp128. They indicated that WB keeps bridging the two Mn ions in the initiation of the reaction because the catalytic activity of Mn-depleted arginase is reduced (*8*). These two mechanisms are schematised in Scheme 1.

As compared to the experimental studies, there are few quantum chemical studies on arginase (*11*–*13*). Ivanov and Klein (*11*,*12*) investigated the geometry in the active site by using DFT and the impact of Asp128 in the case of wild-type and metal-depleted arginase by *ab initio* molecular dynamics. Very recently, Leopoldini et al. (*13*) demonstrated the catalytic mechanism of wild-type and metal-depleted arginases by using hybrid DFT (B3LYP) according to the mechanism proposed by Christianson and his co-workers (*9*,*10*).

In the present study, we elucidate the chemical species of WB in the initial structure by comparing the calculated structural and magnetic property with experimental ones. In addition to the chemical species of WB, it is important whether the magnetic interaction is associated with the hydrolysis reaction. In order to make this point clear, we investigate the pathway of the interaction with the use of natural orbital (NO) analyses and chemical indices. The $J_{ab}$ value of arginase inhibited by NOHA, whose X-ray crystallographic structure is also available, is estimated to

*Corresponding author. Email: tsaito@chem.sci.osaka-u.ac.jp

ISSN 1061-0278 print/ISSN 1029-0478 online

DOI: 10.1080/10610278.2010.506552
http://www.informaworld.com

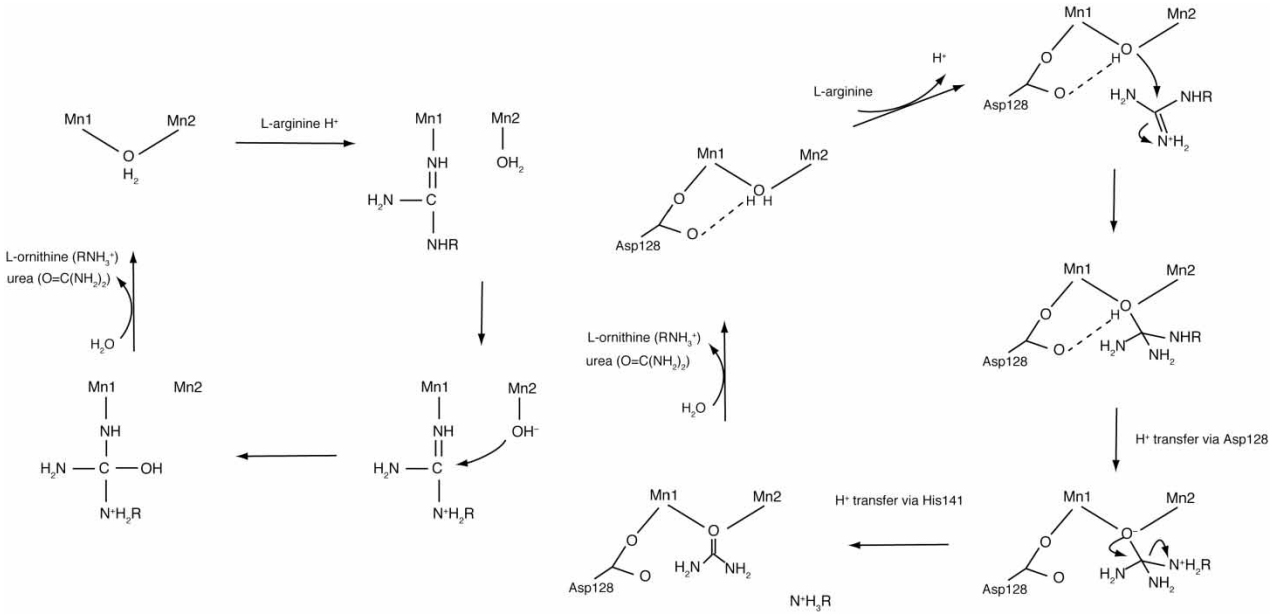


Scheme 1. Proposed EPR-based (a) and structure-based (b) mechanism for the hydrolysis reaction.



confirm the present model size and computational methods.

## 2. Theoretical background

### 2.1 Approximate spin-projection (AP) method

The AP method is based on a local spin expression on Heisenberg Hamiltonian (*14*,*15*):

$$\hat{H} = -2\sum_{a<b} J_{ab}\hat{S}_a\hat{S}_b, \tag{1}$$

where $\hat{S}_a$ and $\hat{S}_b$ represent spin operators at sites $a$ and $b$, respectively. $J_{ab}$ is called an effective exchange integral, and it is equivalent to a magnetic coupling constant. By using a simple approximation that the spin contamination error for a high spin (HS) state is negligibly small, the $J_{ab}$ value can be expressed as follows:

$$J_{ab} = \frac{E^{\mathrm{BS}} - E^{\mathrm{HS}}}{\left\langle \hat{S}^2 \right\rangle^{\mathrm{HS}} - \left\langle \hat{S}^2 \right\rangle^{\mathrm{BS}}}, \tag{2}$$

where $E^{(X)}$ and $\langle \hat{S}^2 \rangle^{(X)}$ denote the total energy and the expectation value of total spin angular momentum for the spin state $X$, respectively.

### 2.2 NO analyses

In order to obtain spin-adapted (SA) picture from the BS solution, the NOs are determined as eigenfunctions of the first-order density matrices

$$\rho(r; r') = \sum n_i \{\phi_i(r)\}^* \phi_i(r'), \tag{3}$$

where $n_i$ denotes the natural orbital occupation number (NOON). NOONs of bonding and anti-bonding NOs are almost 2.0 and 0.0, respectively. The NOONs value is an important index to analyse the spin–orbital interactions. $\psi_i^+$ and $\psi_i^-$ represent the BS MOs:

$$\psi_i^{\pm} = \cos\theta_i\phi_i \pm \sin\theta_i\phi_i^*. \tag{4}$$

where $\theta$ is the mixing parameter between the SA bonding $\phi_i$ and anti-bonding $\phi_i^*$. The corresponding NOONs ($n_i^+$ and $n_i^-$) are given by the orbital overlap $T_i$ between the corresponding orbital pairs:

$$n_i^{\pm} = 1 \pm T_i, \tag{5}$$

where

$$T_i = \left\langle \psi_i^+ | \psi_i^- \right\rangle = \cos 2\theta. \tag{6}$$

The orbital overlap $T_i$ represents degree of covalency of the chemical bond, i.e. $T_i$ becomes 1.0 in the case of the covalent bond, whereas it is 0.0 for the complete diradical (*16*). The NOONs of the BS solution contain important information to understand the nature of chemical bonds in quasi-degenerate systems. The diradical character ($Y_i$) is introduced by using orbital overlap $T_i$ as follows:

$$Y_i = 2W_{\mathrm{D}} = 1 - \frac{2T_i}{1 + T_i^2}, \tag{7}$$

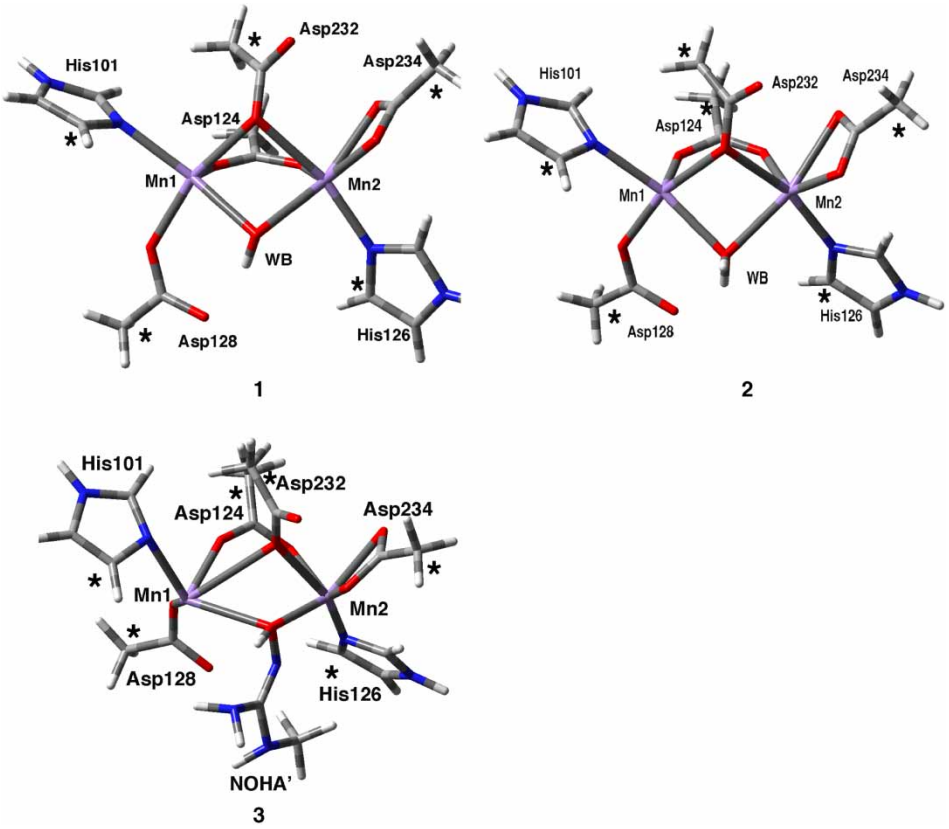


Figure 1. Model complex **1**–**3**. The atoms marked by asterisk were kept fixed during the optimisation.

where $W_D$ denotes the weight of double excitation for orbital *i*. In this way, the bond nature of binuclear transition metal complexes and degrees of electron correlation effect can be related to each other by NO analyses (*17*–*20*).

## 3. Computational details

According to the X-ray crystallographic structure (PDB code: 1RLA) (*2*), we constructed two model complexes **1** and **2** corresponding to WB = $\mu$-$OH^-$ and $\mu$-$H_2O$ as

Table 1. Optimised structural parameters[a] of model **1**.

| | | UB3LYP | | UBH&HLYP | |
|---|---|---|---|---|---|
| Parameters | Expt. | HS | BS | HS | BS |
| *r*(Mn1–Mn2) | 3.32 | 3.05 | 3.02 | 3.06 | 3.04 |
| *r*(Mn1–O) | 2.36 | 2.03 | 2.03 | 2.04 | 2.03 |
| *r*(Mn2–O) | 2.42 | 2.07 | 2.06 | 2.08 | 2.07 |
| ∠Mn1–O–Mn2 | 88.0 | 96.0 | 95.5 | 96.0 | 95.8 |
| *r*(O–Asp128) | 2.81 | 2.85 | 2.83 | 2.88 | 2.87 |
| *r*(Mn1–Asp124) | 2.03 | 2.17 | 2.17 | 2.16 | 2.16 |
| *r*(Mn2–Asp124) | 2.05 | 2.27 | 2.27 | 2.25 | 2.25 |
| *r*(Mn1–Asp232) | 2.29 | 2.23 | 2.22 | 2.22 | 2.22 |
| *r*(Mn2–Asp232) | 2.46 | 2.24 | 2.26 | 2.22 | 2.24 |
| *r*(Mn1–His101) | 2.25 | 2.33 | 2.33 | 2.33 | 2.33 |
| *r*(Mn2–His126) | 2.09 | 2.31 | 2.32 | 2.30 | 2.30 |
| *r*(Mn1–Asp128) | 2.13 | 2.13 | 2.13 | 2.12 | 2.12 |
| *r*(Mn2–Asp234) | 2.39 | 2.21 | 2.22 | 2.22 | 2.22 |
| *r*(Mn2–Asp234′) | 2.11 | 2.34 | 2.34 | 2.31 | 2.31 |

[a] In Å for distances and degrees for angles.

Table 2. Optimised structural parameters[a] of model **2**.

| | | UB3LYP | | UBH&HLYP | |
|---|---|---|---|---|---|
| Parameters | Expt. | HS | BS | HS | BS |
| *r*(Mn1–Mn2) | 3.32 | 3.22 | 3.23 | 3.26 | 3.26 |
| *r*(Mn1–O) | 2.36 | 2.31 | 2.31 | 2.31 | 2.32 |
| *r*(Mn2–O) | 2.42 | 2.37 | 2.36 | 2.34 | 2.34 |
| ∠Mn1–O–Mn2 | 88.0 | 87.0 | 87.4 | 88.7 | 88.8 |
| *r*(O–Asp128) | 2.81 | 2.52 | 2.52 | 2.52 | 2.52 |
| *r*(Mn1–Asp124) | 2.03 | 2.14 | 2.13 | 2.13 | 2.12 |
| *r*(Mn2–Asp124) | 2.05 | 2.16 | 2.16 | 2.15 | 2.15 |
| *r*(Mn1–Asp232) | 2.29 | 2.13 | 2.12 | 2.11 | 2.11 |
| *r*(Mn2–Asp232) | 2.46 | 2.19 | 2.21 | 2.20 | 2.20 |
| *r*(Mn1–His101) | 2.25 | 2.25 | 2.24 | 2.25 | 2.25 |
| *r*(Mn2–His126) | 2.09 | 2.26 | 2.26 | 2.25 | 2.25 |
| *r*(Mn1–Asp128) | 2.13 | 2.08 | 2.09 | 2.08 | 2.08 |
| *r*(Mn2–Asp234) | 2.39 | 2.18 | 2.18 | 2.18 | 2.18 |
| *r*(Mn2–Asp234′) | 2.11 | 2.24 | 2.24 | 2.24 | 2.23 |

[a] In Å for distances and degrees for angles.

Table 3. Calculated Mulliken spin populations on Mn1, Mn2 and O(WB) atoms for **1**–**3**.

| Model | Method | Structure | Spin state | Spin density | | |
|---|---|---|---|---|---|---|
| | | | | Mn1 | Mn2 | O (WB) |
| **1** | UB3LYP | BS | BS | 4.97 | −4.90 | 0.03 |
| | | | HS | 4.86 | 4.85 | 0.15 |
| | | HS | BS | 4.97 | −4.89 | 0.03 |
| | | | HS | 4.87 | 4.84 | 0.14 |
| | UBH&HLYP | BS | BS | 5.00 | −4.91 | 0.02 |
| | | | HS | 4.91 | 4.87 | 0.10 |
| | | HS | BS | 5.00 | −4.91 | 0.02 |
| | | | HS | 4.91 | 4.87 | 0.09 |
| **2** | UB3LYP | BS | BS | 4.91 | −4.87 | 0.00 |
| | | | HS | 4.83 | 4.85 | 0.00 |
| | | HS | BS | 4.92 | −4.87 | 0.01 |
| | | | HS | 4.83 | 4.85 | 0.00 |
| | UBH&HLYP | BS | BS | 4.93 | −4.90 | 0.00 |
| | | | HS | 4.85 | 4.89 | 0.00 |
| | | HS | BS | 4.93 | −4.90 | 0.00 |
| | | | HS | 4.86 | 4.89 | 0.00 |
| **3** | UB3LYP | X-ray | BS | 5.02 | −4.91 | 0.01 |
| | | | HS | 4.97 | 4.83 | −0.01 |
| | UBH&HLYP | X-ray | BS | 4.91 | −4.93 | 0.01 |
| | | | HS | 4.88 | 4.92 | −0.01 |



illustrated in Figure 1. The model complex inhibited by NOHA (PDB code: 1HQF) **3** was also constructed (*9*). NOHA is simplified in **3** as illustrated in Figure 1.

All the calculations were performed at UB3LYP and UBH&HLYP levels of theory (*21*–*24*). The geometry optimisations were performed for the BS ($S = 0$) and HS ($S = 5$) states together with MIDI + p (53321/5321/41) basis sets for Mn (*25*) and 6-31G* basis sets for the other atoms. As shown in Figure 1, the atoms marked by asterisk were kept fixed during the optimisation. Then, we performed the single-point energy calculations by using larger basis sets: MIDI + pd (53321/5321/411) ($\alpha = 0.105$) basis sets for Mn (*25*,*26*) and 6-31 + G** basis sets for the others. The magnetic coupling constant ($J_{ab}$) values and chemical indices (*T*,*Y*) were calculated based on the obtained electronic structures of the BS and HS states.

Table 4. Calculated total energies, $\langle S^2 \rangle$ values and $J_{ab}$ values for **1**–**3**.

| Model | Method | Structure | BS | | HS | | $J_{ab}$[a] |
|---|---|---|---|---|---|---|---|
| | | | Energy | $\langle S^2 \rangle$ | Energy | $\langle S^2 \rangle$ | |
| **1** | UB3LYP | HS | −3744.13512 | 4.9897 | −3744.13379 | 30.0059 | −11.7 |
| | | BS | −3744.13529 | 4.9878 | −3744.13374 | 30.0059 | −13.6 |
| | UBH&HLYP | HS | −3743.26455 | 5.0003 | −3743.26397 | 30.0053 | −5.1 |
| | | BS | −3743.26457 | 5.0000 | −3743.26392 | 30.0054 | −5.7 |
| **2** | UB3LYP | HS | −3744.67801 | 4.9998 | −3744.67755 | 30.0056 | −4.0 |
| | | BS | −3744.67815 | 4.9994 | −3744.67761 | 30.0056 | −4.7 |
| | UBH&HLYP | HS | −3743.81204 | 5.0031 | −3743.81183 | 30.0052 | −1.8 |
| | | BS | −3743.81199 | 5.0031 | −3743.81177 | 30.0052 | −1.9 |
| | Expt.[b] | X-ray | | | | | ∼ −2.0[c] |
| **3** | UB3LYP | X-ray | −3987.77794 | 5.0966 | −3987.79961 | 30.0911 | −1.2 |
| | UBH&HLYP | X-ray | −3986.77469 | 5.0107 | −3986.77463 | 30.0113 | −0.5 |
| | Expt.[d] | X-ray | | | | | ∼0[e] |

[a] In $cm^{-1}$.
[b] From Ref. (*2*).
[c] From Ref. (*3*).
[d] From Ref. (*9*).
[e] From Ref. (*4*).

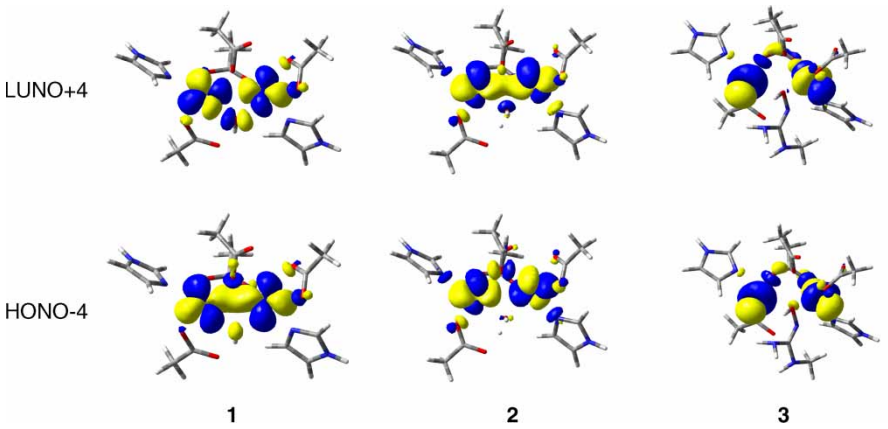


Figure 2. HONO-4 and LUNO + 4 of **1**–**3**.

## 4. Results and discussions

### *4.1 Optimised geometry*

The structural parameters of the X-ray and the optimised structures for **1** and **2** are summarised in Tables 1 and 2.

As for **3**, an optimised structure was not obtained because the N–OH bond cleavage occurred during the optimisation step. Therefore, we performed only single-point calculations based on the X-ray crystallographic structure. The optimised parameters of **1** and **2** do not depend on the spin state and exchange-correlation functionals. The result supports that the spin contamination error caused by the HS state on the electronic

Table 5. Calculated *T* and *Y* values based on NOs for **1**–**3**.

| Model | Method | Structure | Orbital | *T* | *Y*[a] |
|---|---|---|---|---|---|
| **1** | UBH&HLYP | BS | HONO-4 | 0.060 | 88.0 |
| | | | HONO-3 | 0.035 | 93.0 |
| | | | HONO-2 | 0.018 | 96.4 |
| | | | HONO-1 | 0.012 | 97.7 |
| | | | HONO | 0.006 | 98.9 |
| | UB3LYP | BS | HONO-4 | 0.110 | 78.2 |
| | | | HONO-3 | 0.067 | 86.7 |
| | | | HONO-2 | 0.035 | 93.0 |
| | | | HONO-1 | 0.022 | 95.7 |
| | | | HONO | 0.008 | 98.4 |
| **2** | UBH&HLYP | BS | HONO-4 | 0.034 | 93.3 |
| | | | HONO-3 | 0.020 | 95.9 |
| | | | HONO-2 | 0.019 | 96.2 |
| | | | HONO-1 | 0.011 | 97.9 |
| | | | HONO | 0.004 | 99.2 |
| | UB3LYP | BS | HONO-4 | 0.060 | 88.1 |
| | | | HONO-3 | 0.036 | 92.8 |
| | | | HONO-2 | 0.035 | 93.1 |
| | | | HONO-1 | 0.018 | 96.4 |
| | | | HONO | 0.008 | 98.7 |
| **3** | UBH&HLYP | X-ray[b] | HONO-4 | 0.016 | 96.8 |
| | | | HONO-3 | 0.016 | 96.9 |
| | | | HONO-2 | 0.008 | 98.3 |
| | | | HONO-1 | 0.001 | 99.8 |
| | | | HONO | 0.000 | 100.0 |
| | UB3LYP | X-ray[b] | HONO-4 | 0.036 | 92.8 |
| | | | HONO-3 | 0.032 | 93.7 |
| | | | HONO-2 | 0.018 | 96.5 |
| | | | HONO-1 | 0.004 | 99.3 |
| | | | HONO | 0.001 | 99.8 |

[a] In %.
[b] From Ref. (*9*).

structures of the BS state is negligibly small. There is not much difference in the metal–ligand distances between the two. By comparing of structural parameters relating to the Mn–O(WB)–Mn core such as the Mn–Mn, Mn–O distances and Mn–O–Mn angle between **1** and **2**, the optimised model **2** is much closer to the X-ray structure. On the other hand, the O(WB)–O(Asp128) hydrogen bond distance is estimated too short for **2**, while **1** reproduces the experimental one. The hybrid DFT methods are relatively capable of describing hydrogen bonding in contrast to van der Waals interactions (e.g. $\pi$–$\pi$ stacking interactions) (*27*,*28*). From the optimised structural parameters, it is somewhat difficult to determine that WB is identified to $H_2O$ in the initial structure.

### *4.2* $J_{ab}$ *value*

Calculated Mulliken spin populations on the Mn–O(WB)–Mn core of **1**–**3** are summarised in Table 3.

The results show that the localised $S = 5/2$ spins at Mn1 and Mn2 are antiferromagnetically and ferromagnetically coupled for the BS and HS states, respectively. The $J_{ab}$ values between two local spins on each Mn atom were calculated by using Equation (2) as summarised in Table 4.

The total energies and the expectation values of total spin angular momentum ($\langle\hat{S}^2\rangle$) for the BS and HS states are also summarised in Table 4. Calculated $J_{ab}$ values of **2** are much closer to the experimental value than those of **1**. The differences between two models are attributed to the Mn–Mn and Mn–O distances, which affects the direct and superexchange interactions. In particular, the $J_{ab}$ values of **2** obtained by UBH&HLYP reproduce the experimental value well. It is well known that UBH&HLYP outperforms UB3LYP when estimating $J_{ab}$ values of transition metal complexes (*19*,*20*). This is true of the magnetic interaction in the Mn–O(WB)–Mn core of the active site in arginase. The $J_{ab}$ values of **3** also show that there is little magnetic interaction between two spin sites in accordance with the experimental data. Therefore, the chemical species of the bridging ligand can also be identified as $H_2O$ with the help of the magnetic interaction. To our knowledge, this is the first quantitative examination to evaluate the magnetic interaction in the active site of arginase.

### *4.3 NO analyses*

A pathway of a magnetic interaction is important as well as the strength of the interaction. Since the orbital overlap $T$ is an indicator of the strength of the magnetic interaction in the Mn–O(WB)–Mn core, the interaction between higher occupied NO (HONO-4) and lower unoccupied NO (LUNO + 4) is dominant. The HONO-4 and LUNO + 4 of **1**–**3** are depicted in Figure 2. The other NOs are depicted in Figures S1–S3 in the Supporting Information. The orbital overlap $T$ and diradical character $Y$ are summarised in Table 5.

In the case of model **1**, the HONO-4 and LUNO + 4 show the direct Mn–Mn interaction and the superexchange interaction between two Mn ions via $OH^-$. The corresponding NOs of **2** represent direct Mn–Mn interaction and the interaction through Asp232. Judging from $T$ values of HONO-4 and $J_{ab}$ values of **1** and **2**, the geometry of the Mn–O(WB)–Mn core reflects the magnetic interaction. Since both the Mn–Mn and Mn–O distances of **1** are shorter than those of **2**, the superexchange interaction through the bridging O atom exists.

In the case of model **2**, the magnetic interaction through Asp232 should be weak as compared to metal–metal interaction. Therefore, the weak but direct $\sigma$–$\sigma$ interaction between two Mn ions is the main source of antiferromagnetic coupling. The NO analyses support that the magnetic interaction of **3** is quite small because there is only the interaction through Asp124. The $Y$ values are nearly 100%, indicating localised spin structure on both the Mn ions. It is also noteworthy that the abolishment of magnetic interaction for **3** is not due to the loss of the superexchange interaction but due to the elongated Mn–Mn distance (3.9 Å). In other words, WB plays a role for keeping the Mn–$\mu$-O(WB)–Mn core rigid rather than mediating superexchange interaction (*29*), and WB does not have to shift to one side at an early stage of the reaction. Considering mutant Asp128 Asn loses catalytic activity (*8*), the mechanism proposed by Christianson and his co-workers seems to be reliable.

In this way, the structural and magnetic property reveals that the chemical species of WB is $H_2O$ in the initial structure. Then, one proton might transfer from the active site before the substrate encounters the active site, and the activated hydroxyl ion attacks the guanidine group of the substrate. This process of the formation of $OH^-$ is a challenging problem in the future work.

## 5. Conclusion

In this study, the chemical species of solvent molecule (WB) between two manganese ions in the active site of arginase is examined by using BS hybrid DFT methods. The calculated magnetic coupling constant ($J_{ab}$) values show the weak antiferromagnetic coupling in the Mn–O(WB)–Mn core. The $J_{ab}$ value of WB = $H_2O$ calculated by UBH&HLYP ($-1.9\,cm^{-1}$) is comparable with the experimental value ($\sim -2.0\,cm^{-1}$), while that of WB = $OH^-$ is slightly larger ($-5.7\,cm^{-1}$). Therefore, $H_2O$ is the most likely candidate for WB in the initial structure. The WB also plays an important role for keeping the geometry of the Mn–O(WB)–Mn core rigid at the early stage of the hydrolysis reaction. Since it turns out that there is poor correlation between the catalytic activity

and the Mn—O bond cleavage, WB should remain in the middle of two Mn ions as Christianson et al. suggested.

## Acknowledgements

T.S. is grateful for the Research Fellowships from Japan Society for the Promotion of Science for Young Scientists (JSPS). This work has been supported by Grants-in-Aid for Scientific Research (KAKENHI) (Nos 19750046 and 19350070) from JSPS and that on Grant-in-Aid for Scientific Research on Innovative Areas (No. 22108515) from the Ministry of Education, Culture, Sports, Science and Technology (MEXT).

## References

(1) Bewley, M.C.; Flanagan, J.M. In *Handbook of Metalloproteins*; Messerschmidt, A., Huber, R., Poulos, T., Wieghardt, K., Eds.; Wiley: Oxford, 2001; p 952.
(2) Kanyo, Z.F.; Scolnick, L.R.; Ash, D.E.; Christianson, D.W. *Nature* **1996**, *383*, 554–557.
(3) Reczkowski, R.S.; Ash, D.E. *J. Am. Chem. Soc.* **1992**, *114*, 10992–10994.
(4) Khangulov, S.V.; Pessiki, P.J.; Braynin, V.V.; Ash, D.E.; Dismukes, G.C. *Biochemistry* **1995**, *34*, 2015–2025.
(5) Khangulov, S.V.; Sossong, Jr, T.M.; Ash, D.E.; Dismukes, G.C. *Biochemistry* **1998**, *37*, 8539–8550.
(6) Custot, J.; Boucher, J.L.; Vadon, S.; Guedes, C.; Dijols, S.; Delaforge, M.; Mansuy, D. *J. Biol. Inorg. Chem.* **1996**, *1*, 73–82.
(7) Custot, J.; Moali, C.; Brollo, M.; Boucher, J.L.; Delaforge, M.; Mansuy, D.; Tenu, J.P.; Zimmermann, J.L. *J. Am. Chem. Soc.* **1997**, *119*, 4086–4087.
(8) Scolnick, L.R.; Kanyo, Z.F.; Cavalli, R.C.; Ash, D.E.; Christianson, D.W. *Biochemistry* **1997**, *36*, 10558–10565.
(9) Cox, J.D.; Cama, E.; Colleluori, D.M.; Pethe, S.; Boucher, J.L.; Mansuy, D.; Ash, D.E.; Christianson, D.W. *Biochemistry* **2001**, *40*, 2689–2701.
(10) Cama, E.; Emig, F.A.; Ash, D.E.; Christianson, D.W. *Biochemistry* **2003**, *42*, 7748–7758.
(11) Ivanov, I.; Klein, M.L. *Proteins* **2004**, *54*, 1–7.
(12) Ivanov, I.; Klein, M.L. *J. Am. Chem. Soc.* **2005**, *127*, 4010–4013.
(13) Leopoldini, M.; Russo, N.; Toscano, M. *Chem. Eur. J.* **2009**, *15*, 8026–8036.
(14) Yamaguchi, K.; Takahara, Y.; Fueno, T. In *Applied Quantum Chemistry*; Smith, V.H., Schaefer, III, H.F., Morokuma, K., Eds.; D. Riedel: Boston, MA, 1986; p 155.
(15) Yamaguchi, K.; Jensen, F.; Dorigo, A.; Houk, K.N. *Chem. Phys. Lett.* **1988**, *149*, 537–542.
(16) Yamaguchi, K. *Chem. Phys. Lett.* **1975**, *33*, 330–335.
(17) Maruno, Y.; Shoji, M.; Koizumi, K.; Nishiyama, Y.; Kitagawa, Y.; Kawakami, T.; Okumura, M.; Yamaguchi, K. *Polyhedron* **2005**, *24*, 2778–2783.
(18) Koizumi, K.; Shoji, M.; Kitagawa, Y.; Ohoyama, H.; Kasai, T.; Yamaguchi, K. *Eur. Phys. J. D* **2006**, *38*, 193–197.
(19) Shoji, M.; Hamamoto, T.; Koizumi, K.; Isobe, H.; Kitagawa, Y.; Takano, Y.; Yamanaka, S.; Okumura, M.; Yamaguchi, K. *Polyhedron* **2005**, *24*, 2701–2707.
(20) Saito, T.; Kitagawa, Y.; Shoji, M.; Nakanishi, Y.; Ito, M.; Kawakami, T.; Okumura, M.; Yamaguchi, K. *Chem. Phys. Lett.* **2008**, *456*, 76–79.
(21) Becke, A.D. *Phys. Rev. A* **1988**, *38*, 3098–3100.
(22) Lee, C.; Yang, W.; Parr, R.G. *Phys. Rev. B* **1988**, *37*, 785–789.
(23) Becke, A.D. *J. Chem. Phys.* **1993**, *98*, 5648–5652.
(24) Becke, A.D. *J. Chem. Phys.* **1993**, *98*, 1372–1377.
(25) Tatewaki, H.; Huzinaga, S. *J. Chem. Phys.* **1979**, *71*, 4339–4348.
(26) Hay, P.J. *J. Chem. Phys.* **1977**, *66*, 4377–4384.
(27) Kristyán, S.; Pulay, P. *Chem. Phys. Lett.* **1994**, *229*, 175–180.
(28) Matsui, T.; Sato, T.; Shigeta, Y.; Hirao, K. *Chem. Phys. Lett.* **2009**, *478*, 238–242.
(29) Shin, H.; Cama, E.; Christianson, D.W. *J. Am. Chem. Soc.* **2004**, *126*, 10278–10284.